Journal of Electroceramics 6:2, 123–134, 2001

Nanoparticles of Barium Hexaferrite by Gel to Crystallite Conversion and their Magnetic Properties

C. SUDAKAR, G.N. SUBBANNA & T.R.N. KUTTY*
Materials Research Centre, Indian Institute of Science, Bangalore 560012, India

Submitted August 17, 2000; Revised December 28, 2000; Accepted January 1, 2001

Abstract. A novel method for the preparation of nanoparticles of barium hexaferrite is realized by the gel-to-crystallite (G-C) conversion method. Here, gels of $Fe(OH)_3 \cdot xH_2O$, $70 < x < 110$, were reacted with $Ba(OH)_2 \cdot 8H_2O$ in ethanol/water medium at 80–95°C yielding the precursor, barium iron (III) oxy hydroxide hydrate which is x-ray amorphous but crystalline by electron diffraction (ED). Thermal analyses showed dehydroxylation of the precursor around 600°C to barium hexaferrite which exhibits ED with spotty ring patterns. Samples heat-treated at 650°C are X-ray crystalline with average particle size of 17 nm, which on recrystallization at 780–930°C gives monocrystallites with spot patterns by ED. By varying the wet chemical conditions, precursors of variable Fe_2O_3/BaO ratios could be prepared which on heat-treatment yield monophasic hexaferrite of Fe_2O_3/BaO ratio ranging from 4.51 to 6. In hyperbarium compositions, annealing at 1350°C leads to ordering of excess barium in anti-BR sites within Ba─O layers of β-alumina type unit cells. Nanoparticles of barium hexaferrite with superparamagnetic as revealed by Mössbauer spectra, the temperature vs. magnetization plots and the absence of hysteresis in B-H curves. With increasing temperature of heat treatment, the area under the B-H loop increases continuously, with the magnetization increasing from 2 to 52 emu/g. The conversion from superparamagnetic to ferrimagnetic state is continuous because of the out-diffusion of cation vacancies, created to charge compensate hydroxyl ions, which, in turn, affects Fe^{3+}-O^{2-}-Fe^{3+} superexchange interactions, with the addition of surface and size factors.

Keywords: gel to crystallite conversion, barium hexaferrite, superparamagnetism, nanoparticles, hyperbarium hexaferrite

1. Introduction

Barium hexaferrite, $BaFe_{12}O_{19}$, a classical ferrimagnetic material, is currently of renewed scientific and technological interest because of its relatively strong anisotropy and moderate magnetization. Some of the areas in which micron to submicron-sized barium hexaferrite powders find important roles are permanent magnets, high-density magnetic and magneto-optic recording media, and microwave tunable devices working at frequencies as high as 70 GHz [1, 2]. In fine particle systems, peculiar magnetic properties can be expected, which are explained through surface effects, particle size and morphology, impurities, or crystallographic defects, which are different from those observed for coarse-grained materials [3]. In any case, the magnetic properties of these materials depend largely on the microstructure, which, in turn, varies with the preparative methods.

Different methods have been developed for the preparation of ultrafine barium hexaferrite particles. These include chemical coprecipitation [4], glass crystallization [5], organometallic precursor routes [6], pyrosol method [7], the sol-gel processing [8]. In essence, small sized particles are sought in order to make the phase conversion from the precursor at as low a temperature as possible. In all the above methods, the constituent ions are first intimately mixed at the atomic level so that subsequent nucleation and crystallization occur at relatively low temperatures. In this way, grain growth is prevented during the phase formation. In addition, these particles are free from

*To whom all correspondence should be addressed.

deleterious strain developed when particle diminution is effected by milling, the process usually employed in fine powder preparation from ceramic routes.

Wet chemical synthesis through gel-to-crystallite (G-C) conversion of ultrafine ceramic powders continues to be a subject of intense research activity as these products exhibit advantages over powders derived from conventional ceramic routes. The preparation of multicomponent ceramic oxides has been well studied by the G-C conversion method [9]. The general reaction involved in this technique is the direct conversion of gel into crystallites under wet-chemical conditions, by the breakdown of the gel network caused by the change in ionic pressure brought about by the chemical influx of aliovalent ions [10, 11]. The main advantages of this method are the increased homogeneity and high surface area of the resulting powders, which lead to relatively high reactivity and hence low sintering temperatures. Furthermore, the raw materials are not expensive. This method has advantages in operational cost and procedural simplicity. Various β-alumina compounds, the closely related structural type of magnetoplumbite, have been synthesized by G-C conversion method [12, 13]. In the present work, barium hexaferrite nano-particles are synthesized by this method, having different Fe_2O_3/BaO mole ratios, with the intention to study the effect of nonstoichiometry in the structure and magnetic properties of this oxide.

2. Experimental

A reactive gel of hydrated ferric hydroxide, $Fe(OH)_3 \cdot xH_2O$, $70 < x < 110$, was prepared by the addition of ammonium hydroxide at 30–40°C to ferric chloride solution until the pH was in the range of 6–8. The gel was washed free of anions and ammonium ions. No special care was taken to control the particle size of the gel. The gel was suspended in $Ba(OH)_2$ solution, in presence of a hydrophilic solvent such as ethanol, taken in a flask fitted with a water-cooled reflux condenser. Air in the vessel was displaced by nitrogen. Fresh entry of CO_2 was prevented by the use of an alkali-guard tube. The reaction was carried out at 80 to 95°C for 4–6 h. The solid phase remaining in the reaction vessel was then filtered, washed free of $Ba(OH)_2$ and air-dried, resulting in the nano-sized crystallite precursor. The latter on thermal treatment at elevated temperatures yielded the hexaferrite phases. Samples were prepared having different Fe_2O_3/BaO mole ratios (represented by '*n*') ranging from 3 to 8.

The quantitative chemical analyses of the products obtained were carried out to confirm the composition by dissolving the precursor or the final product. The solution (mother liquor) remaining after recovering the solid product was also analyzed for the unreacted $Ba(OH)_2$. Iron was estimated by direct titration with EDTA, using salicylic acid as the indicator, at the pH of 3 to 4. Barium was estimated by gravimetric analysis, as $BaSO_4$.

Phase identification of the powders was carried out by X-ray powder diffraction (Scintag/USA diffractometer using Cu-Kα radiation). Thermal analysis was performed on a simultaneous thermogravimetry/differential thermal analyzer (TG-DTA) from Polymer Laboratory, STA 1500, at a heating rate of 10°C min^{-1}. Further, the isothermal weight loss studies were carried out by the thermal annealing of larger quantities (grams) of samples at chosen temperatures. Infrared absorption spectra were recorded on a Perkin-Elmer infrared spectrometer in the range 4000 to 300 cm^{-1} by mounting the sample in anhydrous KCl pellets. Electron diffraction and microscopy were carried out with a JEOL, JEM 200CX, transmission electron microscope (TEM) for morphological and lattice imaging studies. Particle size and shape were evaluated by the intercept method. The magnetic susceptibility and the ferrimagnetic transformations were monitored by a home-built Guoy balance having variable temperature facility. To study the magnetization with respect to the applied field, a Vibrating Sample Magnetometer (VSM, Lakeshore, USA) was used. Mössbauer spectra were recorded at constant acceleration in conjunction with a Nuclear Data Instruments ND60 multichannel analyser using a ^{57}Co source in a rhodium matrix. The experimentally observed Mössbauer spectra were curve-fitted by a least-squares method by computer, assuming Lorentzian line shapes.

3. Results

During the initial stages of the gel-to-crystallite conversion, the $Fe(OH)_3 \cdot xH_2O$, gel, a sticky, voluminous mass, disintegrates by the influx of Ba^{2+} ions. As the reaction proceeded, the gel lost its appearance and was converted into flowing powdery mass in presence of the solvent. The solid product so obtained after washing and oven drying was a fine, weakly agglomerated

powder. This precursor powder, barium iron (III) oxyhydroxide, was found to be x-ray amorphous but crystalline by electron diffraction.

3.1. Thermal Analysis

TG-DTA traces of the precursor are shown in Fig. 1(a). Thermal analysis shows that there are three TG steps with an overall weight loss of 14–15% in the range of 25–1000°C. The differential thermo gravimetric (DTG) curve (Fig. 1(c)) shows clearly three regions of weight loss marked by the minima. The first weight loss below 100°C (∼7%), associated with an endothermic DTA peak arises from the loss of water retained even in the oven-dried sample. The second weight loss around 300°C is due to dehydroxylation and the third one extending up to 600°C is due to further dehydroxylation. The weight loss is completed by about 600°C. The presence of water as well as hydroxyl groups in the precursor are very clear as no other constituents than H_2O is identified in the evolved gas analysis. Presence of H_2O as well as OH groups are confirmed by infrared spectra of the samples heated at 200 to 400°C (Fig. 2). The isothermal weight loss experiments (with no discernible endothermic peak in DTA) suggest that the conversion of the precursor to the hexaferrite around 450–650°C is a kinetically controlled thermal decomposition process. The exothermic peak at 780–930°C with no weight loss stems from the recrystallization followed by grain growth of particles. It has been observed from TEM micrographs that rapid grain growth of particles is associated with change in morphology from spherical to acicular crystallites around these temperatures. The exothermic peak shifts to higher temperature (930°C) for the samples prepared with water alone as the reaction medium (Fig. 1(b)). This reflects higher retention of hydroxyl ions by the samples prepared from water-rich medium. The difference is also seen at the

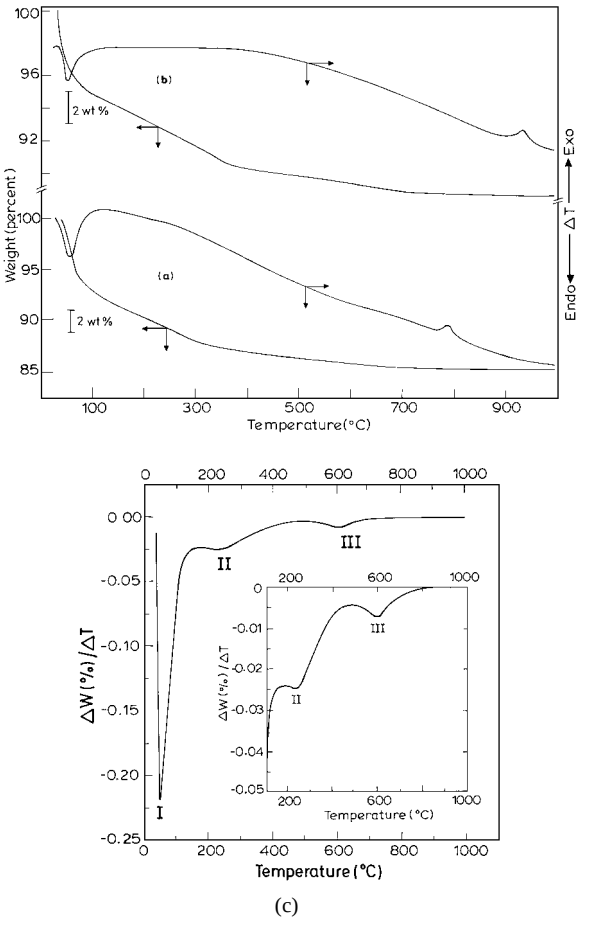

(c)

Fig. 1. TG-DTA traces of barium hexaferrite precursors prepared using (a) ethanol/water (=0.6) medium (b) using water medium (c) DTG curve of TG plot in (a).

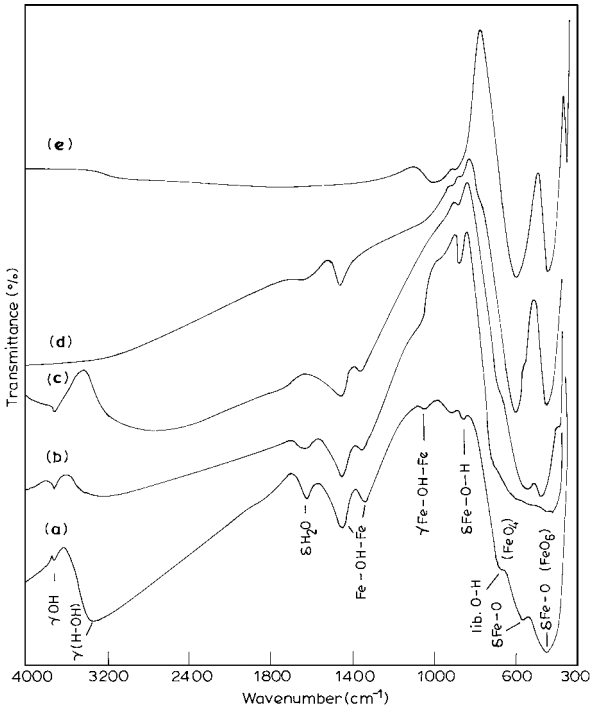

Fig. 2. IR absorption spectra of barium hexaferrite precursor after heating at different temperatures for 6 h. (a) as-prepared, (b) 200°C, (c) 400°C, (d) 950°C, and (e) 1100°C.

third stage of weight loss, mostly due to dehydroxylation, which extends up to 700°C.

In order to establish the composition of the precursor, isothermal weight loss was carried out around the temperature range at which changes were noticed in TG-DTA curves. The sample was maintained at the desired temperatures until constant mass was obtained. Complete weight loss was observed around 600°C. The powder on heat treatment at >650°C becomes hexaferrite with no formation of other intermediate phases (for $4.51 < n < 6$). From the above observation the following reaction sequence can be envisaged in the formation of barium hexaferrite (for $n = 6$).

$$12Fe(OH)_3{\cdot}xH_2O(gel) + Ba(OH)_2$$
$$\xrightarrow[\text{Ethanol}+H_2O]{75-90^\circ C} BaFe_{12}O_{15.71}(OH)_{6.58}{\cdot}7H_2O$$
$$\xrightarrow{\geq 200^\circ C} BaFe_{12}O_{15.71}(OH)_{6.58}\,(\text{Precursor}) + 7H_2O$$
$$\xrightarrow{>600^\circ C} BaFe_{12}O_{19}\,(\text{Hexaferrite}) + 3.29H_2O$$

3.2. *Effect of Fe_2O_3/BaO Ratio (n) and Ethanol/Water Ratio*

The BaO content in the precursor obtained from the G-C conversion increases with the decrease in Fe_2O_3/BaO mole ratio (n) in the reaction mixture. When 'n' is between 4.5 to 6, the precursor yields hexaferrite phase on annealing above 650°C. For Fe_2O_3/BaO ratio greater than 6, hematite and for Fe_2O_3/BaO ratio less than 4.5, $BaFe_2O_4$ are formed as the additional phases. The chemical compositions of the precursor and the ferrite phases obtained upon calcination at 850°C are given in Table 1. The prehistory of the sample such as, (i) precipitation conditions (temperature, pH and concentration of the solution) and (ii) aging of the gel, which affect the network nature of the gel, also have effect on the precursor. To avoid larger variations in the preparation, controlled precipitation conditions were followed. Ferric chloride solution (0.08 molar) in distilled water at a temperature ∼40°C was precipitated at the pH ≈8, with no aging of the gel, which resulted in lower recrystallization temperatures and nearly spherical particle morphology.

The effect of varying ethanol/water (solvent ratio, S.R.) ratio was studied with initial Fe_2O_3/BaO ratio maintained around 4. The water retained in the gel, ca. 95% by weight, was released and no additional water was introduced whereas ethanol content was varied. The uptake of Ba^{2+} ions by the solid was not found to vary with the S.R. However the temperature of decomposition of the precursor (i.e. the temperature of hexaferrite phase formation, as identified by x-ray powder diffraction) on heat treatment was affected by the S.R. When the S.R. was 0.6, the lowest ferrite recrystallization temperature was 650°C. For S.R. <0.6, the ferrite recrystallization temperature increases to 800°C. Further, the gel-to-crystallite reaction conducted with water as the reaction medium showed increased ferrite recrystallization temperature (850°C). This difference in ferrite recrystallization temperature is attributed to the variation in crystallite size of the product, which is affected by the changing network nature and stability of the gel for different preparative conditions. The difference in the OH^- contents in the precursor, in turn, brings out differences in the temperature of crystallization of hexaferrite. Thus the samples were prepared, for

Table 1. Chemical compositions of the various products.

$n = Fe_2O_3/BaO$ (mole)			
In reactants (G-C conversion)	In products	Chemical composition (As prepared specimens)	Phases identified after heating at 850°C[a]
8.00	8.22	$Ba_{0.73}Fe_{12}O_{15.73}(OH)_6\ 5.9H_2O$	H, α
6.67	6.82	$Ba_{0.88}Fe_{12}O_{16.12}(OH)_{5.52}\ 5H_2O$	H, α
5.88	6.00	$BaFe_{12}O_{15.71}(OH)_{6.58}\ 7H_2O$	H
4.62	4.92	$Ba_{1.22}Fe_{12}O_{16.47}(OH)_{5.5}\ 6.5H_2O$	H
4.00	4.51	$Ba_{1.33}Fe_{12}O_{16.08}(OH)_{6.5}\ 7H_2O$	H
3.43	3.82	$Ba_{1.57}Fe_{12}O_{17.17}(OH)_{4.8}\ 4.4H_2O$	H, B
3.00	3.33	$Ba_{1.8}Fe_{12}O_{17.55}(OH)_{4.5}\ 4.8H_2O$	H, B

[a]H = hexaferrite; $\alpha = \alpha$-Fe_2O_3; B = $BaFe_2O_4$.

further analyses, with the liquid medium having the S.R. ∼0.6.

3.3. Infrared Spectra

In order to identify the presence of OH^- groups, IR spectra of samples ($n = 6$) heat- treated at different temperatures are taken (Fig. 2). The as-prepared sample shows a broad absorption band centered at 3324 cm^{-1} corresponding to the hydrogen bonded O─H stretching. Absorption band due to the bending mode of H_2O molecule around 1620 cm^{-1} is diagnostic of the presence of water of hydration. The sharp band in the O─H stretching frequency region, around 3730 cm^{-1}, indicates the presence of independent ionic OH groups or the hydroxyl group without hydrogen bonding. The absorption band around 659 cm^{-1} arises from the librational (breathing) mode of OH^- groups. Absorption bands around 1450–850 cm^{-1} region arrive from the stretching modes of FeO_4 as well as Fe─OH─Fe groups [14]. The absorption band around 1063 cm^{-1} is assigned to the stretching mode of Fe─OH─Fe groups and that at 849 cm^{-1} is due to the bending vibrations of Fe─O─H [15]. The absorption band at 1440 cm^{-1} is due to the vibrations of Fe─OH─Fe groups wherein each OH group is bridged to the neighbouring Fe(III) ions.

The sample heat treated at 400°C shows the absence of an absorption band corresponding to hydrogen bonded O─H stretching (3324 cm^{-1}), the bending mode of H_2O (1620 cm^{-1}) and the librational mode of OH group (659 cm^{-1}). Also the absorption band around 1063 cm^{-1} due to the stretching mode of Fe─OH─Fe disappeared and the bending vibration of Fe─OH around 849 cm^{-1} with decreased intensity is discernible. However, the O─H stretching band (3730 cm^{-1}) still persists after heating at this temperature. The samples heated at 650°C as well as <950°C show weak absorption bands at 1450 cm^{-1} and 853 cm^{-1} corresponding to the vibrations of Fe─OH─Fe groups. These cannot be due to carbonate group (such as $BaCO_3$) as the 1100°C heated sample shows the absence of these bands (Fig. 2), whereas the absorption bands due to $BaCO_3$ ought to have persisted.

3.4. X-Ray Powder Diffraction

The oven-dried (∼100°C) precursor is X-ray amorphous and so are the samples heated below 600°C.

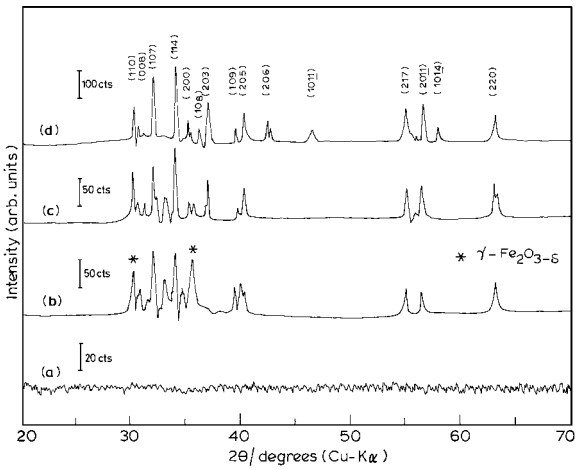

Fig. 3. XRD patterns of sample ($n = 6$) heat treated at (a) 200°C and 650°C for (b) 6 h, (c) 12 h, and (d) 24 h.

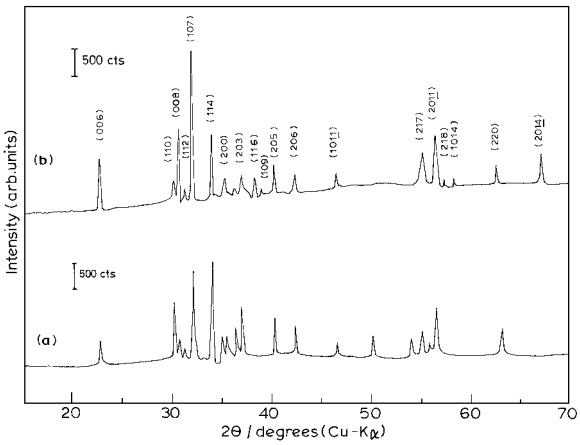

Fig. 4. XRD patterns of samples ($n = 6$) heat treated at (a) 850°C (powder sample), and (b) 1350°C (sintered sample).

From TG, the completion of weight loss around 600°C suggests that the dehydroxylation is effective around 600°C. This is followed by recrystallization and the increase in grain size, which is dependent on the duration of heating at ≥650°C. X-ray diffraction patterns for the sample ($n = 6$) heat-treated at various temperatures and duration are shown in Figs. 3 and 4. The XRD pattern for the sample heat-treated at 650°C for 6 h correspond to that of the hexaferrite phase (Fig. 3(b)). The minor peaks marked in Fig. 3(b) are due to γ-$Fe_2O_{3-\delta}$ having the defect-spinel

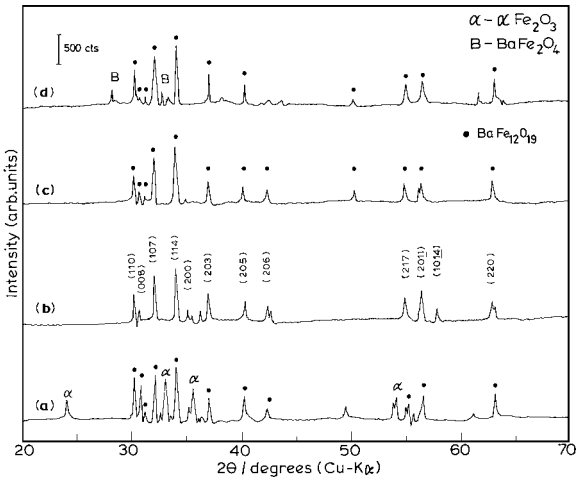

Fig. 5. XRD patterns of samples with Fe_2O_3/BaO ratio of (a) $n = 8.22$, (b) $n = 6$, (c) $n = 4.51$, and (d) $n = 3.33$, heat treated at 850°C. (Counts are same for all patterns).

structure (common peaks appear for $BaFe_{12}O_{19}$ of (110) plane and $\gamma-Fe_2O_{3-\delta}$ of (220) plane at $2\theta = 31.3°$). These low intensity peaks are not observed in samples prepared with $n < 6$. With increase in duration of heating to >12 h these lines vanish and the diffraction pattern is characteristic of single phase M-type barium hexaferrite. Thus the minor phase of defect-spinel is a transient intermediate found in low concentration from the precursor. Under higher barium ion concentration ($n < 6$) the precursor transforms directly to hexaferrite without any transient intermediate. It is significant to note that X-ray reflections from no other possible phases such as $BaCO_3$, α-Fe_2O_3, $BaFe_2O_4$ are seen in the diffraction pattern confirming the phase-purity of the product. Even in the samples heated at 1350°C (Fig. 4), where the segregation of minor phases ought to be faster and complete, no additional XRD peaks are noticed. This confirms the unique advantage of the preparative method. The difference in the intensity of peaks, for example, between (110), (008), (107) and (114), of 850°C heated powder sample and 1350°C sintered ceramics are due to the preferential growth of certain crystallographic planes of the grains in the sintered specimens. The lattice parameters calculated from XRD ($a = 5.898$ Å, $c = 23.20$ Å) are in good agreement with the reported values [16].

X-ray diffractograms of the samples heat-treated at 850°C for 6 h, with varying Fe_2O_3/BaO mole ratios (n) are shown in Fig. 5. For $n > 6$ the presence of hematite, α-Fe_2O_3 is identified whereas for $n < 4.5$, $BaFe_2O_4$ along with the hexaferrite phase has been detected. For $4.5 < n < 6$ there is excess barium retained in the precursor even after thorough washings. On heating these precursors no phases other than hexaferrite have been identified in X-ray diffractogram. The samples with $4.5 < n < 6$ heat-treated at 1350°C show only hexaferrite with no segregation of other phases. The lattice parameters calculated from XRD for $n = 4.51$ ($a = 5.894$ Å; $c = 23.34$ Å) show slight variations from those of $n = 6$ composition. The formula unit of the precursor calculated from the chemical composition and the phases identified for different 'n' values are given in Table 1. M-type hexaferrites with hyper-stoichiometry in barium, have indeed been reported [17]. Also, refined crystal structure of non-stoichiometric M-type hexagonal ferrite is known, with the excess barium located on the mirror plane at the anti-BR (Beevers-Ross) positions and on O_4 layers of spinel block, substituting for oxygen atoms in Ba-rich β-alumina type cell [18].

3.5. TEM Studies

The precursor powders were found to be X-ray amorphous but crystalline by electron diffraction. The ED pattern (Fig. 6(c)) from a finely dispersed region showed rings made up of discrete spots due to nanocrystalline particles of size ~10 nm determined by the intercept method from the micrograph (Fig. 6(a)). The transmission electron micrographs of samples ($n = 6$) heated at 650°C (12 h) show nanocrystallites of 17 nm average size (Fig. 6(b)). The electron diffraction patterns of these crystallites show ring patterns superimposed with spots, revealing polycrystallinity of individual crystallites and also confirm the formation of hexaferrite phase. The average particle size increases with annealing temperature and duration; thus the average particle size of 650°C (24 h) heated sample is 22 nm. A typical lattice image corresponding to the layered structure of hexaferrite obtained on one of the crystallites is shown in the inset of Fig. 6(b). The spacing between successive white fringes is 11.6 Å corresponding to one half of the magnetoplumbite unit cell along the c-axis.

The acicular morphology of these particles starts developing upon heating beyond 850°C. These observations are noted commonly for both the stoichiometric ($n = 6$) and samples with hyper-barium ($n = 4.51$) contents. A typical bright field image of the latter sample is shown in Fig. 7(a). The aspect

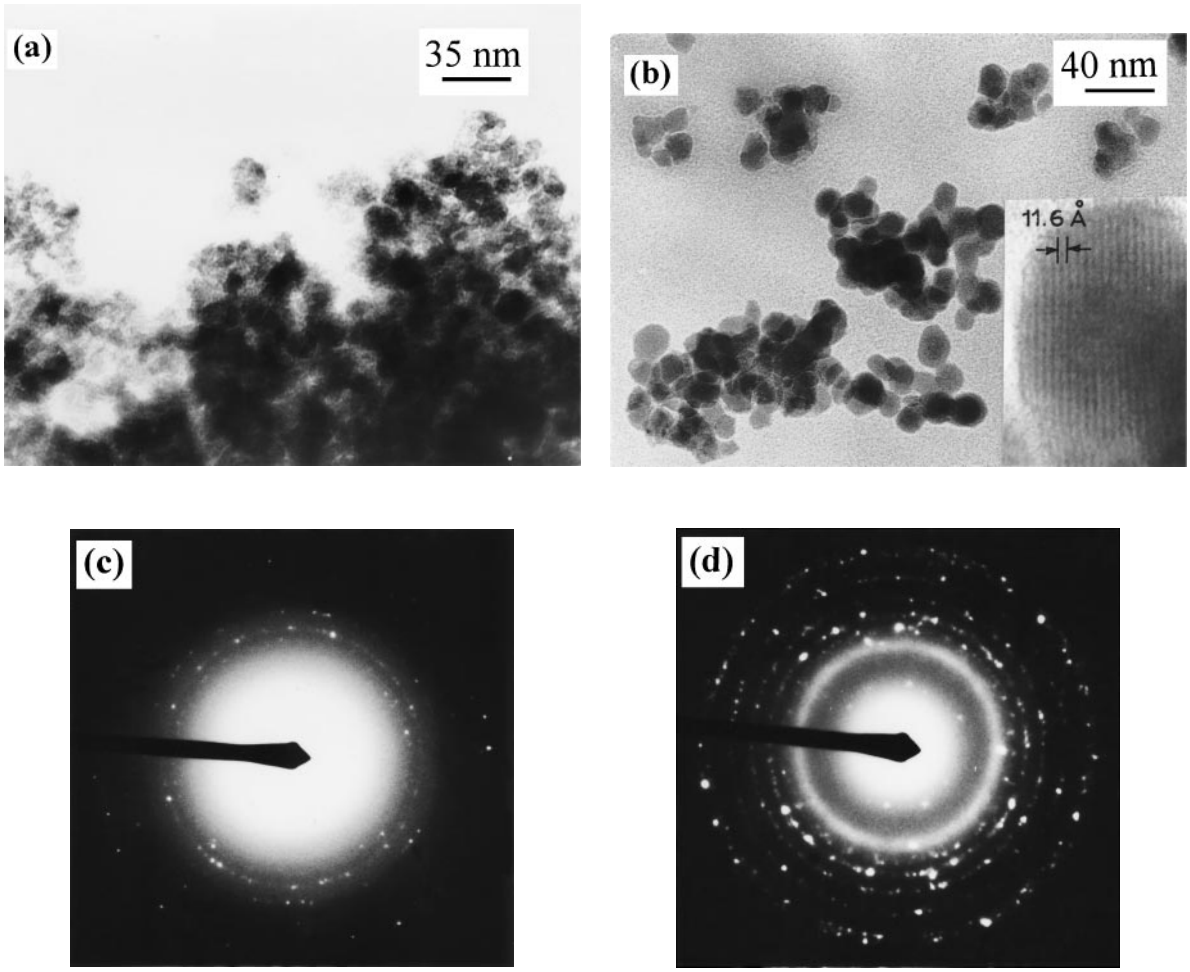

Fig. 6. TEM micrographs of (a) 300°C and (b) 650°C heated sample. The corresponding electon diffraction patterns of (a) and (b) are shown in (c) and (d). The lattice image of a particle is shown in the inset of (b).

(length/breadth) ratio is in the range of 2 to 5. The selected area electron diffractions of these particles are invariably spot patterns indicating that they are monocyrstallites. The lattice image of a crystal with the beam parallel to [100] direction is shown in Fig. 7(b). The corresponding selected area diffraction pattern is shown in the inset of Fig. 7(b). There are no intergrowths seen as revealed by the high resolution electron microscopy (HREM).

Samples with $n = 4.51$, heat-treated at 1350°C, exhibit superlattice reflections. The electron diffraction patterns of both stoichiometric and hyper-barium content samples heat treated at 1350°C, taken with incident electron beam normal to (001) plane, are shown in Fig. 8(a) and (b). The bright spots in both the patterns are basal reflections of hexaferrite phase. However, for the hyper-barium samples, weak spots are observed, situated at $h = k = n/2$, where 'n' is an integer. This result suggests the presence of a2*a2 superstructure. Such electron diffraction patterns are not observed for samples heat-treated at temperatures <1300°C as the barium ordering may not be taking place or is destroyed at that temperature. The lattice relationship between the magnetoplumbite type subcell and the supercell are $A_1 = 2a_1$, $A_2 = 2a_2$ and $C = nc_0$, where 'n' is an integer and A_1, A_2 and C are lattice vectors for the supercell and a_1, a_2 and c_0 for the subcell. The ordering along C axis is not known. If it is equal to the subcell, the superstructure cell volume will be fourfold that of the subcell.

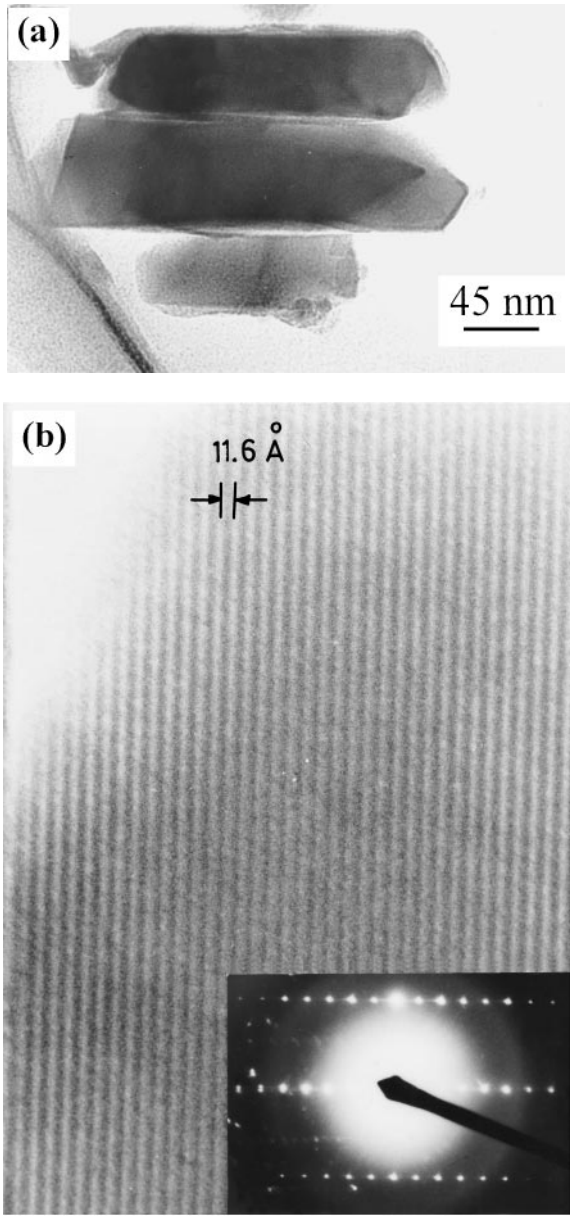

Fig. 7. (a) Bright field image of fully-grown acicular particles ($n = 4.51$). (b) lattice image of one of the acicular particles recorded along [100]. The electron diffraction pattern is shown in the inset.

3.6. Magnetic Measurements

The temperature vs. magnetization curves for the samples ($n = 6$) heat-treated at different temperatures are shown in Fig. 9. With the increase in the heat-treatment temperature, magnetization increases at room temperature. The 650°C (12 h) heated sample, where the phase formation is complete with the average particle size of 17 nm, shows similar behaviour as that of 200°C heat-treated sample. The samples heat-treated at 650°C have low magnetization values, notwithstanding they are hexaferrites, and exhibit superparamagnetic property. The samples heat-treated at 750 to 1050°C shows ferrimagnetic behaviour with the room temperature magnetization increasing with increase in heat-treatment temperature. These magnetizations are not saturation values as the measurements are carried out at lower fields, because barium hexaferrite has a very high anisotropy field of the order of 16 kOe [19]. However, the effective anisotropy field for single domain

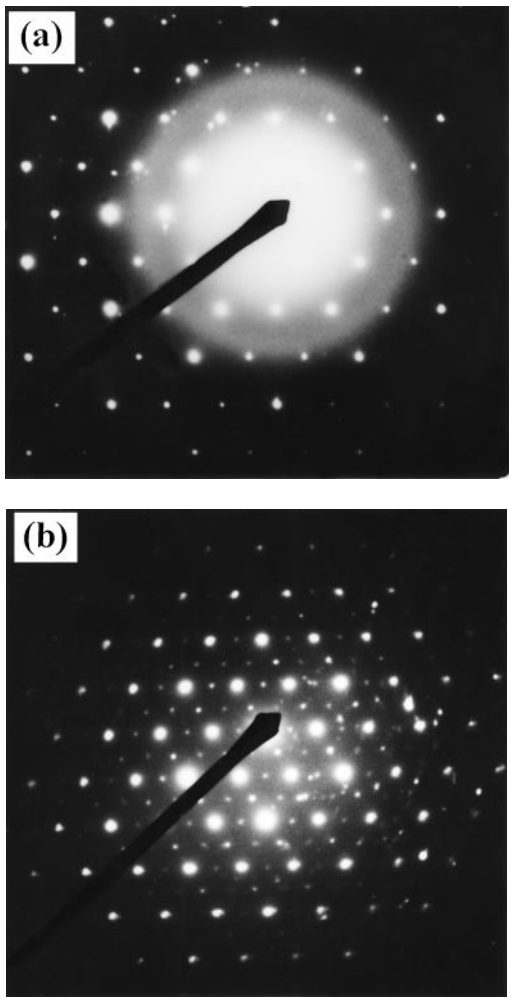

Fig. 8. Electron diffraction pattern of (a) $n = 6$, and (b) $n = 4.51$ with the electron beam normal to (001) plane.

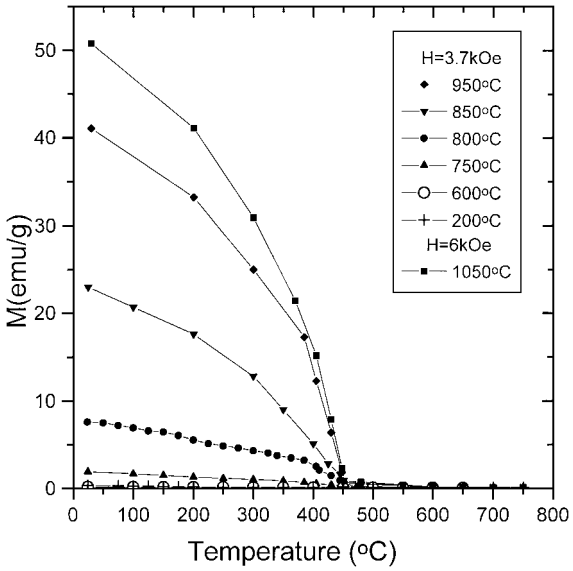

Fig. 9. Magnetization vs. Temperature curves for cooling cycle of sample ($n = 6$) heat-treated at different temperatures.

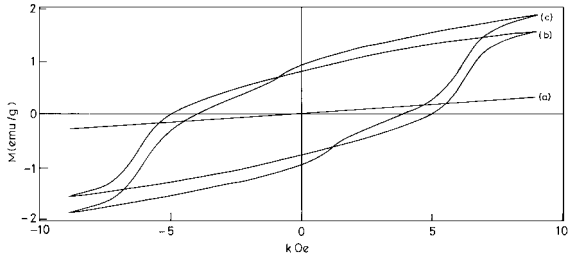

Fig. 10. Magnetization vs applied magnetic field curves for samples heat-treated at (a) 650°C ($n = 6$ or $n = 4.51$), (b) 750°C ($n = 6$) and (c) 750°C ($n = 4.51$).

particles of $BaFe_{12}O_{19}$ depends on the shape and thickness of the particles [19, 20]. The results indicate that the conversion of superparamagnetic particles to ferrimagnetic ones is not all at once. The conversion takes place over a range of temperature.

The variation of magnetization as a function of applied magnetic field (with the maximum applied field of 10 kOe) is shown in Figs. 10 and 11. The 650°C (12 h) heated sample shows linear variation with the applied field, with no apparent saturation magnetization. The threshold size for the superparamagnetic behaviour is very small in barium hexaferrite, around 10 nm [21], which suggests that large fraction of the presently prepared particles are superparamagnetic in nature although they are of 17–22 nm range according to TEM studies. The Mössbauer spectra of the sample heat-

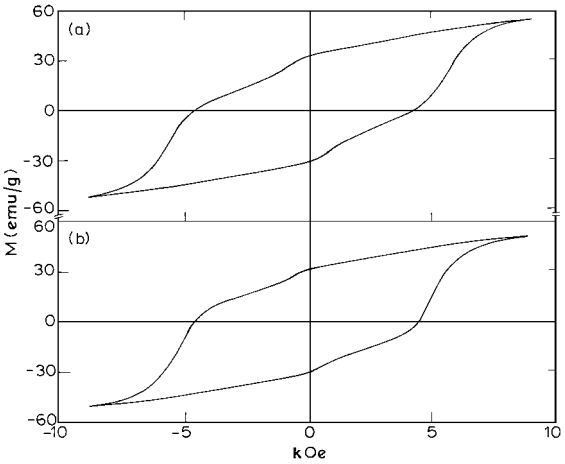

Fig. 11. Magnetization vs. applied magnetic field curves of sample (a) $n = 6$ and (b) $n = 4.51$ heat-treated at 950°C.

treated at 650°C exhibit a doublet characteristic of superparamagnetic behaviour of particles (Fig. 12). The 750°C heat-treated samples show hysteresis behaviour, with the coercivity of 4.987 kOe but having lower specific magnetization of 1.56 emu/g. The 950°C heat-treated sample shows both coercivity and near specific saturation magnetization ($H_c = 4.52$ kOe; $\sigma_s = 52.01$ emu/g). Generally the saturation magnetization is less than 72 emu/g measured for bulk material of $BaFe_{12}O_{19}$ at room temperature [22] and values of σ_s reported for small $BaFe_{12}O_{19}$ particles, prepared by several different methods are given by Haneda et al. [19]. In the present preparations, σ_s approaches near saturation above 9 kOe as the hysteresis loop tapers off at higher field strengths (Fig. 11). Yamada et al. [23] have pointed out that the saturation magnetization of $BaFe_{12}O_{19}$ small particles diminishes with decreasing particle size. The Mössbauer spectra of 950°C heat-treated sample exhibit multiplets characteristic of barium hexaferrites (Fig. 12).

Coercivity, H_c of small particles is expected to increase with reduction in particle size until single-domain particles are reached and then decreases as the superparamagnetic limit is approached [19, 24]. Interestingly, in the present preparation of particles the coercivity for 750°C and 950°C heat-treated samples remain in the range of 4.5 to 5 kOe (Figs. 10 and 11), and differs from the existing reports observing decrease in coercivity with decrease in particle size below the value of single domain particle size [19, 24]. A similar behaviour was found for samples

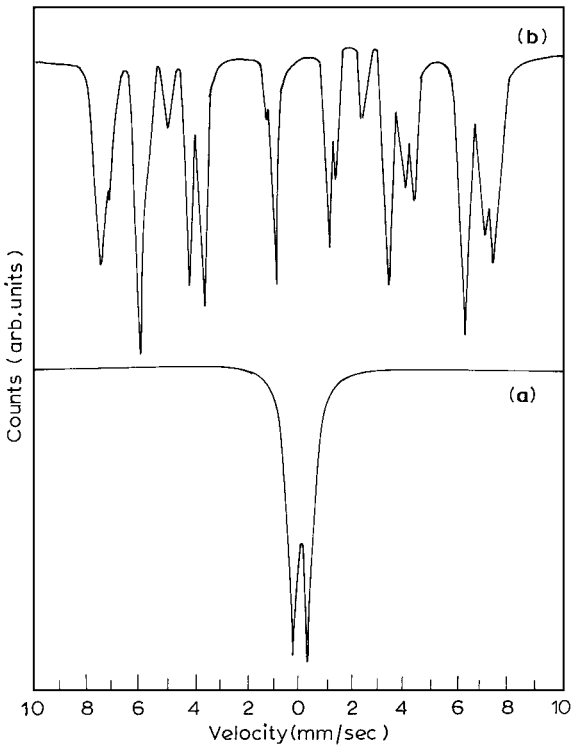

Fig. 12. Room temperature Mössbauer spectra of barium hexaferrite heat-treated at (a) 650°C for 6 h and (b) 950°C for 24 h.

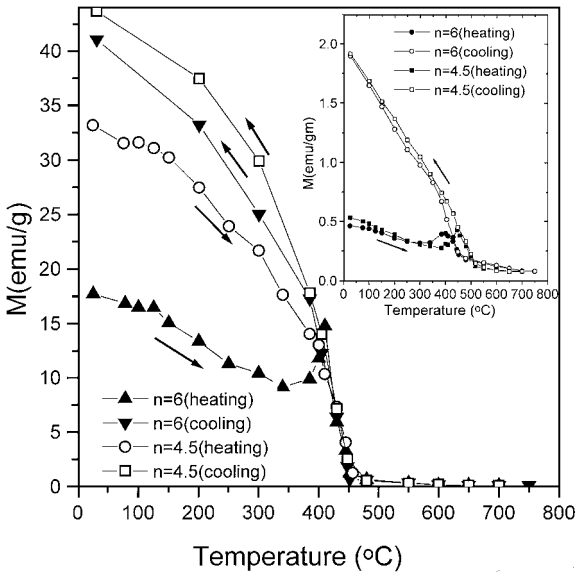

Fig. 13. The heating and cooling cycles of magnetization vs. temperature curves for samples ($n = 6$ and 4.5) heat-treated at 950°C and 750°C (inset) measured at the field of 3.7 kOe.

with $n = 4.51$. The 650°C heated samples are superparamagnetic, the 750°C heated sample showing high H_c and low σ_s ($H_c = 3.94$ kOe; $\sigma_s = 1.856$ emu/g) and 950°C heated sample showing higher H_c and σ_s ($H_c = 4.57$ kOe; $\sigma_s = 50.65$ emu/g).

The temperature vs. magnetization curves at an applied field of 3.7 kOe, for both heating and cooling cycles of samples ($n = 6$, 4.51) heat-treated at 750°C and 950°C are shown in Fig. 13. The magnetization first decreases with temperature, reaches a minimum and then increases to a maximum before decreasing again sharply to approach zero. However in the cooling curves such maxima are not observed and the magnetization increases monotonically during cooling with much larger magnetization. This is due to the fact that at higher temperature the magnetic moments of the particles switch easier into field direction than at lower temperature. This behaviour is typical of the Hopkinson effect reported for single-domain particles of barium ferrite and predicted theoretically earlier [25–27]. The shift in the observed maximum to higher temperature is seen for hyperbarium sample ($n = 4.51$) heat treated at 750°C. However such a maximum is not observed for the same samples heat-treated at 950°C. There are two competing effects for the change in magnetization of samples with increasing temperature. The first is a decrease in spontaneous magnetization of each particle, which brings about a decrease in sample magnetization. At the same time the magnetocrystalline anisotropy also decreases, which leads to increase in magnetization due to easier reorientation of particles. In 950° heated sample ($n = 4.51$) the latter effect does not overcome the former and hence no maximum is realized. However the cooling curve shows increased magnetization due to irreversible rotation of magnetic moments. The observation of Hopkinson effect is consistent with the observation of B-H hysteresis of samples heat-treated at 750°C exhibiting ferrimagnetic behaviour showing the partial conversion from superparamagnetic state to the ferrimagnetic state.

The Curie temperatures (T_c) of samples heat-treated at 950°C, calculated from $1/\chi$ vs. temperature plots, are 453 ± 5°C ($n = 6$) and 463 ± 5°C ($n = 4.51$) which is close to T_c of bulk barium hexaferrite samples. However, for 750°C heated samples, T_c values were found to be ~390°C ($n = 6$) and 440°C ($n = 4.51$), in spite of the particle size being the same for both samples. Thus the presence of excess barium influences

the T_c to reach close to that of the bulk value, even for samples heat-treated at lower temperatures.

4. Discussion

Gel-to-Crystallite conversion is a general technique used for the preparation of nanosized multinary oxides such as aluminates, ferrites, zirconates, titanates, etc. [9]. The general feature of the gel-to-crystallite (G-C) conversion involves the instability of the metal hydroxide gel brought about by the disruption of the ionic pressure in the gel as a result of the faster diffusion of A^{2+} ions (more electropositive constituent in multinary oxides) through the solvent cavities within the gel framework. This is accompanied by the splitting of bridging groups such as B-(OH)-B or B-O-B (where B is the less electropositive or transition metal constituent) leading to chemical rearrangements. This causes the breakdown of the gel into fine crystalline particles. It is inevitable that OH^- ions are retained randomly in the place of O^{2-} ions. The presence of lattice OH groups has been observed by IR spectra. Hydroxyl groups escape from the crystallites as H_2O after the heat treatment. The basic mechanism involved in the formation of multinary oxides may be the deolation of the bridging groups such as B-(OH)-B and B-O-B followed by oxolation in $B^{n+}O_{n/2}$ and are charge compensated by the A^{2+} ions leading to a stable multinary oxide lattice. It is inevitable that OH^- ions are retained in the place of O^{2-} ions. The presence of OH groups has been observed by IR spectra. Hydroxyl groups escape from the crystallites as H_2O after heat treatment. These residually retained OH^- ions are charge compensated by the formation of cation vacancies. Since the system accommodates excess barium in the structure, the cation vacancies are due to the absence of Fe^{3+} ions. Presence of OH^- ions at O^{2-} sites together with the cation vacancies affect Fe^{3+}-O^{2-}-Fe^{3+} superexchange interaction, further disrupting the long range cooperative interactions in samples heat treated at $<600^\circ$C. Thus the thermal randomization of spins is inevitable in these samples. Residual hydroxyl ions are liberated for samples heat-treated at higher temperatures; however the size and surface factors along with the cation vacancies control the behaviour of particles. The cation vacancies are removed only after heating above the recrystallization temperatures. Thus, the 650°C heated sample is in the superparamagnetic state, although the size of the particles (17–22 nm) is higher than the reported critical size for superparamagnetic state ($\sim$10 nm) [21]. With further increase in heat treatment temperature the particle size increases and becomes ferrimagnetic on cooling. The conversion from superparamagnetic to ferrimagnetic state is not an abrupt one but takes place over a range of temperature. This can be seen from the gradual increase of σ_s from 2 emu/g for 750°C heated sample to 52 emu/g for 950°C heated sample.

One experimentally observed composition for excess barium M-ferrite is $Ba_{1.33}Fe_{12}O_{19.33}$. No intergrowths are seen for this sample. Thus, on the basis of the electron diffraction patterns observed (Fig. 8(b)) and the excess Ba postulated in the formula, the ordering of such excess Ba ions may take place within the Ba-O layers of β-alumina type subcell. The excess Ba ions enter into anti-BR sites to avoid interactions with Ba ions at BR sites. Barium occupying one out of three kinds of the anti-BR sites for each Ba─O layer accounts for the approximate 1/3 excess Ba ions in the formula [28]. No ordering along *C*-axis is discernible by TEM studies, indicating that the stacking sequence of the layers containing the excess Ba ions (excess Ba-O layers) is random.

A theory to explain the Hopkinson effect in single-domain particles has been proposed [25, 26]. The existence of a Hopkinson maximum in the thermomagnetic curves could be connected with the process of irreversible rotation of magnetic moments. Such processes become possible with the decrease in the magnetocrystalline anisotropy upon heating. The present observation supports the theory of Hopkinson effect proposed for single-domain particles of barium ferrite [27].

5. Conclusions

The preparation of fine particles of barium hexaferrite was accomplished by Gel-to-Crystallite conversion method by the present studies. Preparation of barium hexaferrite with Fe_2O_3 to BaO ratio (n) of 4.5 to 6 was realized. The presence of hydroxyls with the associated cation vacancies in the hexaferrite samples, disrupt the long-range cooperative interactions. Thus, the particles evolve from the paramagnetic state of the precursor to the metastable state exhibiting superparamagnetic behaviour for 650°C heat-treated

samples due to nanosizes of fine particles as well as due to the crystal defects and to multidomain ferrimagnetic crystallites after heating to higher temperatures. Further, on sintering the particles recrystallise with subsequent grain growth and acquire bulk ferrimagnetic characteristics. Thus the size and surface factor along with the defects due to cation vacancies control the magnetic properties of the nanoparticles. The excess barium (for $n = 4.5$) is accommodated in the anti-BR sites within Ba─O layers of β-alumina type unit cell. However, no correlation of the occupied anti-BR sites between excess Ba─O layers is observed. Further, various ferrimagnetic oxides possessing structures closely related to hexaferrites can be prepared by this method by partially substituting the Fe^{3+} sites with divalent/trivalent transition metal ions.

References

1. M.P. Sharrock and L. Josephson, *IEEE Trans. Magn.*, **22**, 723 (1986); T. Fujiwara, *IEEE Trans. Magn.*, **23**, 3125 (1987); M.P. Sharrock, *IEEE Trans. Magn.*, **25**, 4374 (1989).
2. M.H. Kryder, *J. Magn. Magn. Mater.*, **83**, 1 (1990); P. Gerard, E. Lacroix, G. Marest, M. Duphy, G. Rolland, and B. Blanchard, *ibid.*, **83**, 13 (1990).
3. V. Ens, in *Ferromagnetic Materials*, Vol. **3**, edited by P. Wohlfarth (North-Holland, Amsterdam, 1982), p. 3.
4. K. Haneda, C. Miyakawa, and H. Kojima, *J. Am. Ceram. Soc.*, **57**(8), 354 (1974).
5. B.T. Shirk and W.R. Buessem, *J. Am. Ceram. Soc.*, **53**, 192 (1970).
6. F. Licci, G. Turilli, and T. Besagni, *IEEE Trans. Magn.*, **24**, 593 (1988).
7. M.V. Cabanãs, J.M. González-Calvet, N. Labeau, P. Mollard, M. Pernet, and M. Vallet-Regí, *J. Solid State Chem.*, **101**, 265 (1992).
8. E. Lucchini, S. Meriani, F. Delben, and S. Paoletti, *J. Mater. Sci.*, **19**, 121 (1984).
9. P. Padmini and T.R.N. Kutty, *J. Mater. Chem.*, **4**(12), 1875 (1994).
10. T.R.N. Kutty and P. Padmini, *Mater. Res. Bull.*, **27**, 945 (1992).
11. M.I. Diaz-guemes, T.G. Carreno, C.J. Serna, and J.M. Palacios, *J. Mater. Sci.*, **24**, 1011 (1989).
12. T.R.N. Kutty, V. Jayaraman, and G. Periaswami, *Mater. Res. Bull.*, **31**, 1159 (1996).
13. V. Jayaraman, G. Periaswami, and T.R.N. Kutty, *J. Mater. Chem.*, **8**(4), 1087 (1998).
14. K. Nakamoto, *Infrared Spectra of Inorganic and Coordination Compounds* (John Wiley & Sons, Inc., 1963).
15. K. Parida and J. Das, *J. Colloid and Interface Sci.*, **178**, 586 (1996).
16. W. Wong-Ng, H. Mcmurdie, B. Daretzkin, C. Hubbard, and A. Dragoo, *Powder Diffraction*, **3**, 249 (1988).
17. M. Najmi, P. Poix, and J.C. Bernier, *J. Phy. (Paris)*, **C8/9**, 839 (1988).
18. A.C. Stergiou, D. Samaras, O. Kalogirou, H. Vincent, and A. Bekka, *Solid State Ionics*, **50**, 11 (1992).
19. K. Haneda and A.H. Morrish, *Phase Transitions*, **24–26**, 661 (1990).
20. K. Haneda and A.H. Morrish, *IEEE Trans. Magn.*, **25**(3), 2597 (1989).
21. V.K. Sankaranarayanan, Q.A. Pankhurst, D.P.E. Dickson, and C.E. Johnson, *J. Magn. Magn. Mater.*, **125**, 199 (1993).
22. B.T. Shirk and W.R. Beussem, *J. Applied Physics*, **40**(3), 1294 (1969).
23. H. Yamada, M. Takano, M. Kiyama, J. Takada, T. Shinjo, and K.Watanabe, *Adv. Ceram.*, **16**, 169 (1985).
24. B.T. Shirk and W.R. Beussem, *IEEE Trans. Magn.*, **MAG-7**, 659 (1971).
25. O. Popov, P. Racher, M. Mikkov, F. Calderon, J.L. Sanchez Ll, and F. Leccabue, *J. Magn. Magn. Mater.*, **99**, 119 (1991).
26. O. Popov and M. Mikhov, *J. Magn. Magn. Mater.*, **75**, 135 (1988).
27. O. Popov and M. Mikhov, *J. Magn. Magn. Mater.*, **82**, 29 (1989).
28. N. Iyi, S. Takekawa, Y. Bando, and S. Kimura, *J. Solid State Chem.*, **47**, 34 (1983).